Modeling and experimental study to identify arrival-time jitter sources in the presence of a magnetic chicane

P. Craievich,* S. Di Mitri, M. Milloch, G. Penco, and F. Rossi
Elettra-Sincrotrone Trieste S.C.p.A. 34149 Basovizza, Trieste, Italy
(Received 12 December 2012; published 5 September 2013)

The accurate and stable synchronization between electron bunch and external laser is a key requirement for the successful operation of an externally seeded free electron laser. This requirement is particularly stringent when the electron bunch is longitudinally compressed to sub-ps durations. We present an analytical description of the electron bunch arrival-time jitter that, supported by experimental evidence, allows the identification of specific, dominant jitter sources. The arrival-time jitter measurements were carried out as a function of the bunch length compression factor in FERMI@Elettra linac. The experimental behavior of the pulse-to-pulse time jitter agrees well both with the analytical predictions and particle tracking simulations. Our modeling takes into account the photoinjector laser arrival time on the cathode, the jitter of phases and voltages of the radio-frequency accelerator, and fluctuations of the compressor's dipole field.

DOI: 10.1103/PhysRevSTAB.16.090401 PACS numbers: 29.20.Ej, 29.27.Eg, 41.75.Ht

I. INTRODUCTION

The FERMI@Elettra free electron laser (FEL) is a single-pass, S-band linac-based externally seeded FEL implementing high gain harmonic generation in the 80-4 nm fundamental output wavelength range. Commissioning started in September 2009, the first FEL output with seeded operation was produced in December 2010, and first light was provided to users in April 2011 [1]. One of the key requirements for guaranteeing a successful operation of this seeded FEL facility has been the stability of the temporal overlap between the electron bunch and the seed laser. The shot-to-shot temporal fluctuation of the seed laser is determined by the laser system stability and by the timing synchronization with the machine reference signal. Currently a rms time jitter of about 50 fs has been measured for the FERMI seed laser [2]. On the contrary, the electron bunch arrival-time jitter (ATJ) is essentially determined by the arrival time of the photoinjector drive laser with respect to the gun rf phase and by the conversion of the energy jitter to the time domain via dispersive elements along the machine.

The main dispersive sections in the FERMI linac are the two magnetic chicanes that are used to longitudinally compress the beam in combination with an off-crest setting of the upstream accelerating structures rf phases. This configuration implies that electron bunch energy jitter at the entrance of the chicane develops into time jitter by means of the momentum compaction $|R_{56}|$. Moreover, fluctuations of the chicane dipoles's magnetic fields leads to beam trajectory fluctuations in the chicane itself and will increase the electron bunch ATJ. Changing the longitudinal compression factor by varying the R_{56} of the chicane or, alternatively, the upstream linac rf phase will each have different consequences for the beam ATJ. In order to optimize the FEL performance, it is important to clearly understand where the major contribution comes from, both to identify and fix eventual systems malfunctioning and to improve the final performances.

We have used the FERMI linac up to the first magnetic chicane (BC1), to investigate the electrons ATJ behavior under several different longitudinal compression configurations. This paper is organized as follows. Section II summarizes the layout of the front end of the FERMI linac, highlighting the location of the important diagnostics relevant to timing jitter. In Sec. III we present an analytical model for describing the behavior of the electrons ATJ after activating the magnetic compression, which takes into account the fluctuations of the chicane bending currents, the upstream rf sections (phases and voltage), and the ATJ of the injector drive laser. A benchmark with a tracking code is presented in Sec. IV that confirms the reliability of the analytical model. Finally Sec. V is dedicated to the measurements of the electrons ATJ versus the compression factor performed in the FERMI linac.

II. LAYOUT

Although the nominal configuration of the FERMI linac includes two stages of magnetic bunch length compression, only the first one, called BC1, was installed at the time of the measurements reported in this paper. Figure 1 shows the major components of the FERMI@Elettra linac up to

*Present address: Paul Scherrer Institute, 5232 Villigen PSI, Switzerland

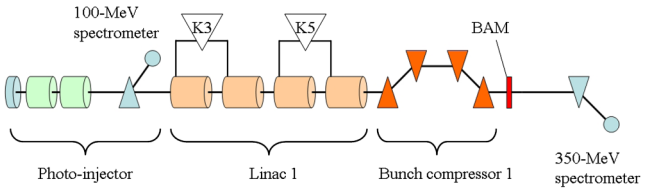

FIG. 1. Schematic layout of FERMI from the gun to the 350 MeV spectrometer line; the bunch arrival monitor is just beyond BC1.

the 350 MeV spectrometer line [3]. A photocathode radio-frequency (rf) gun is followed by 2 S-band (2998 GHz) accelerating structures, providing a 100 MeV, up to 800 pC single electron bunch at the repetition rate of 10 Hz [4]. Linac 1 consists of 4 S-band, 4.5-m long accelerating structures with one klystron driving two accelerating structures. BC1 is a movable, 4-dipole symmetric chicane that allows a continuously tunable bending angle in the range 0–122 mrad. The maximum magnetic chicane momentum compaction $|R_{56}|$ provided by the system is 96 mm.

III. ANALYTICAL MODEL FOR THE ARRIVAL-TIME JITTER

The electron bunch ATJ is defined as the short-term time-of-flight variation of its center of mass relative to the time of flight of a (virtual) reference particle. The reference time of flight is determined by the nominal setting of the accelerator and magnetic lattice as well as by specific initial conditions in the longitudinal phase space for the reference particle. We assume pure longitudinal acceleration in the rf sections so that the energy gain of each electron is a function of the sampled rf phase ϕ and can be written as $E = E_i + eV\sin(\phi)$, with E_i representing the electrons energy at the injector exit and considering the maximum energy gain for $\phi = \pi/2$. Only linear dispersive motion with no energy change is considered in the chicane, which is characterized by a R_{56} linear transport matrix element. The chicane is assumed to be achromatic, symmetric, and made of four identical dipole magnets that are powered by the same power supply in order to produce the same magnetic field B. For such a geometry and small bending angle, $\theta \ll 1$, the matrix element R_{56} is

$$R_{56} \approx -2\theta^2\left(\frac{2}{3}l_1 + l_2\right), \tag{1}$$

where l_1 is the dipole rectilinear magnetic length and l_2 is the distance between the first (third) and second (fourth) dipole magnet edge along the longitudinal beam axis. The electron beam is assumed to be ultra-relativistic; thus the longitudinal charge distribution is frozen in the straight sections. Our analysis excludes any considerations about the particle transverse phase space and frictional forces.

We adopt the bunch centroid as the reference particle. Its final time coordinate in the laboratory frame can be written as

$$t_f = t_i + \frac{\Delta l + l_d}{c}, \tag{2}$$

where t_i is the reference initial arrival time, l_d is the straight trajectory length (zero bending angle), and Δl is the path length difference between the beam trajectory through the chicane and the straight trajectory, namely [5],

$$\Delta l = 4l_1\left(\frac{\theta}{\sin\theta} - 1\right) + 2l_2\left(\frac{1}{\cos\theta} - 1\right). \tag{3}$$

If $\theta \ll 1$, we can use the following approximation:

$$\Delta l \approx \theta^2\left(\frac{2}{3}l_1 + l_2\right) \approx -\frac{R_{56}}{2}. \tag{4}$$

In order to evaluate the arrival-time jitter of the bunch centroid after the chicane, we differentiate Eq. (2) with respect to the particle energy and the magnetic field B:

$$dt_f = dt_i + \frac{d(\Delta l)}{c} = dt_i + \frac{\partial(\Delta l)}{\partial E}dE + \frac{\partial(\Delta l)}{\partial B}dB. \tag{5}$$

In the following we evaluate the partial derivatives in Eq. (5) taking advantage of the relationship $l_1 = \rho\sin\theta$ with $\rho = E/cB$ the bending radius:

$$\frac{\partial(\Delta l)}{\partial E} = \frac{\partial(\Delta l)}{\partial\theta}\frac{\partial\theta}{\partial E} \approx \frac{R_{56}}{E} \tag{6}$$

and

$$\frac{\partial(\Delta l)}{\partial B} = \frac{\partial(\Delta l)}{\partial R_{56}}\frac{\partial R_{56}}{\partial\theta}\frac{\partial\theta}{\partial B} \approx -\frac{R_{56}}{B}. \tag{7}$$

A beam energy variation at the entrance of the chicane is mainly due to fluctuations of the rf phase ϕ, the amplitude V, and the arrival time from the injector. By differentiating the particle energy E with respect to V, ϕ, and t_i, it follows that

$$dE = e\sin\phi dV + eV\cos\phi d\phi + eVck\cos\phi dt_i, \tag{8}$$

where k is the rf wave number. By substituting Eqs. (6)–(8) in Eq. (5), we finally obtain

$$dt_f \approx dt_i + \frac{R_{56}}{c}\left(\frac{e\sin\phi}{E}dV + \frac{eV\cos\phi}{E}d\phi + \frac{eVck\cos\phi}{E}dt_i - \frac{dB}{B}\right). \tag{9}$$

We consider the one-stage bunch length compression factor in the linear approximation,

$$C = \frac{1}{1 + hR_{56}}, \tag{10}$$

where h is the so-called linear energy chirp:

$$h = \frac{1}{E}\frac{dE}{dz} = \frac{eVk\cos\phi}{E_i + eV\sin\phi}. \quad (11)$$

Substituting Eqs. (10) and (11) in Eq. (9) we obtain

$$dt_f \approx \frac{dt_i}{C} + \frac{R_{56}}{c}\left(\frac{e\sin\phi}{E}dV + \frac{eV\cos\phi}{E}d\phi - \frac{dB}{B}\right). \quad (12)$$

As already mentioned, the arrival-time jitter at the injector exit dt_i is dominated by the drive laser arrival-time jitter relative to the gun rf phase. In the absence of any jitter source after the injector, dt_i is compressed for a negative R_{56} because an earlier (later) arrival of the bunch centroid to the rf field, which translates into an earlier (later) arrival at the finish point, implies a lower (higher) energy at the chicane and therefore a longer (shorter) path length with respect to the reference trajectory. Consequently, the initial time jitter is exactly reduced by the compression factor C, as shown in Eq. (12). It is worthwhile noting that contribution from linear energy-chirp jitter due to mean energy jitter at the injector exit and rf amplitude and phase jitters in linac 1 are negligible relative to the other terms in Eq. (12). Furthermore, in this analytical model we have excluded contribution at the ATJ due to the bunch length jitter at the injector exit as it is small compared to the terms in Eq. (12) and as it is also reduced by the compression factor after the chicane.

All jitter sources described above are considered to be small and independent perturbations to the particle motion, so the electron bunch ATJ after the chicane is obtained by summing all the terms in quadrature:

$$\Sigma_t^2 \approx \left(\frac{\sigma_{t_1}}{C}\right)^2 + \left(\frac{R_{56}}{c}\right)^2\left[\left(\frac{\sigma_B}{B}\right)^2 + \left(\frac{E_{L_1}}{E}\right)^2\left(\frac{\sigma_V}{V}\right)^2 + \left(\frac{eV\cos\phi}{E}\right)^2\sigma_\phi^2\right], \quad (13)$$

where E_{L_1} is the energy gain in linac 1 at the rf phase ϕ. A similar formula is also presented in [6]. The term due to rf phase jitter in Eq. (13) plays a crucial role during the bunch length compression. With regard to this, we plot the ATJ as a function of the linac 1 rf phase in Fig. 2, assuming the same phase for all the accelerating structures. In Fig. 2, ATJ is evaluated for several values of the rf phase jitters and two specific values of the injector exit rms time jitter, 80 fs and 150 fs, respectively. We assumed a relative amplitude jitter for linac 1 of 0.02% and a chicane magnets rms current jitter of 0.01%. For small values of the rf phase jitter, the stronger the compression factor is, the smaller the ATJ is. In case of a larger rf phase jitter, the ATJ behavior versus the rf phase presents a minimum. This latter gradually moves towards $\phi = \pi/2$ ($C = 1$) and it increases when the rf phase jitter inreases. This effect is more evident in the presence of a small injector exit time jitter, so if this latter is very small the requirement on the rf phase stability becomes even more stringent. Similarly, Fig. 3 shows the ATJ versus the linac 1 rf phase for several values of the

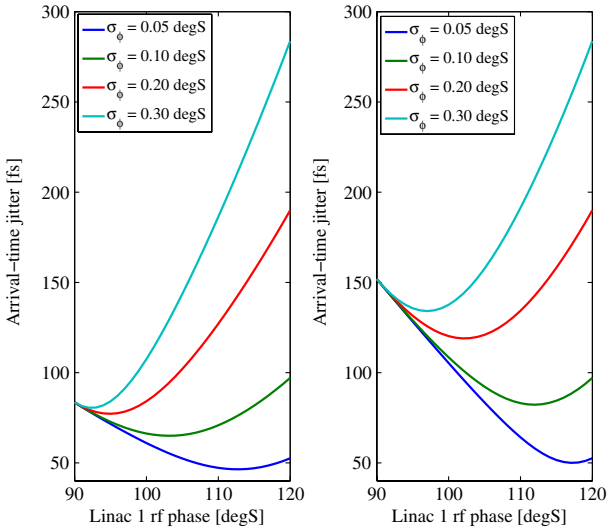

FIG. 2. $dV/V = 0.02\%$, $dB/B = 0.01\%$, $R_{56} = -41$ mm. Injector exit rms time jitter 80 fs (left) and 150 fs (right).

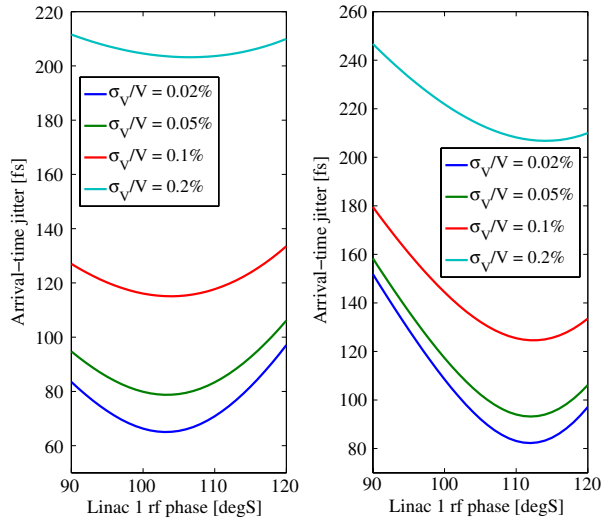

FIG. 3. $\sigma_\phi = 0.1°$, $dB/B = 0.01\%$, $R_{56} = -41$ mm. Injector exit rms time jitter 80 fs (left) and 150 fs (right).

relative amplitude jitters of the linac 1, where the injector exit rms time jitter was set again to 80 fs and 150 fs. The rms rf phase jitter is 0.1° and the magnets rms current jitter is 0.01%. With increasing linac amplitude jitter, all ATJ curves shift towards higher values. The local minimum, however, remains observable but the position of the minimum relative to the compression factor only depends on the linac 1 rf phase jitter and on the ATJ at the injector exit.

IV. TRACKING CODE RESULTS

In this section we present a comparison between the analytical prediction for the ATJ and particle tracking results obtained with the LiTrack [7] code. An rf phase jitter for the linac 1 of 0.1° and 0.3° was chosen, respectively. The rms jitter of the linac 1 phases and voltages and

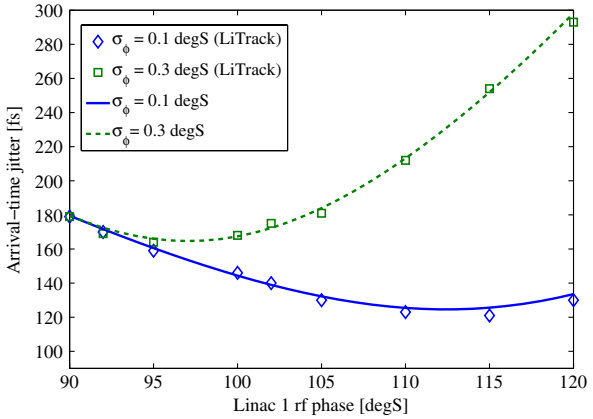

FIG. 4. $dV/V = 0.1\%$, $dB/B = 0.01\%$, $R_{56} = -41$ mm. Initial time jitter: 150 fs.

the R_{56} chicane parameter were adopted as input to LiTrack in a statistical study that used Latin hypercube sampling [8]. Analysis of the global output parameters provided an estimation of the ATJ. Figure 4 shows the statistical results over 400 different configurations of the accelerator, at constant bunch charge and assuming $\sigma_{t_i} = 150$ fs and $\sigma_V/V = 0.1\%$. LiTrack simulations results are in good agreement with the analytical approach described above and in fact both predict an ATJ minimum at the same rf phase.

V. EXPERIMENTAL RESULTS

The nominal FERMI rf amplitude and phase values, their required short-term stability tolerances, and their measured stability are listed in Table I [9,10]; basically the short-term stability tolerances for the FERMI linac have been achieved for each rf system. Figs. 5 and 6 show some representative amplitude and phase jitter measurements.

Figure 7 shows the bunch mean energy jitter at the injector exit measured over 20 seconds at 10-Hz sample rate. It is worthwhile noting that the rms value is 0.014%

TABLE I. Nominal settings, rms short-term stability tolerances, and measured rms values of the rf amplitudes, rf phases, charge and initial arrival-time jitter (Δt_i) for the FERMI bunch compression system.

Parameter	Nominal value	rms tolerance	measured rms	rms unit
L1 rf amplitude (K3)	125 MV	0.1	0.018	%
L1 rf phase (K3)	115°	0.08	0.056	degS
L1 rf amplitude (K5)	125 MV	0.1	0.020	%
L1 rf phase (K5)	115°	0.08	0.063	degS
R_{56}	−41 mm	0.02	0.02	%
Charge	300 pC	4	2	%
Δt_i		350	60–80	fs

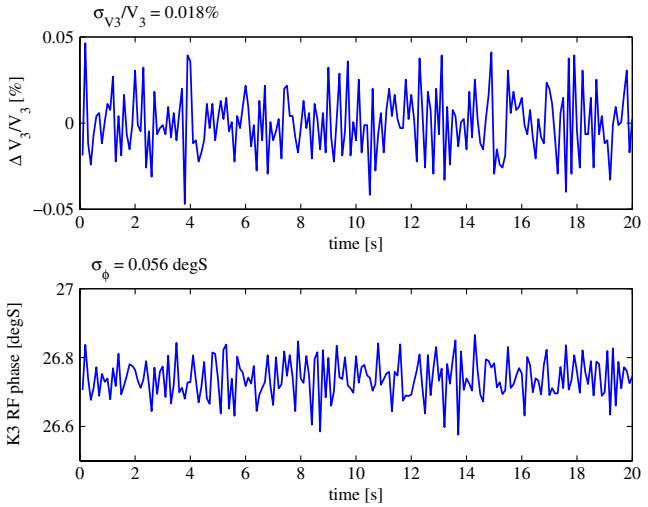

FIG. 5. The relative rf amplitude (top) and rf phase jitter (bottom) of the K3 klystron in L1 rf section measured over 20 sec at a 10 Hz sample rate (feedback active).

and this fluctuation will not be taken into account in the analytical model.

In order to experimentally investigate the ATJ behavior as a function of the compression factor, we systematically added artificial noise to the rf signal by means of the Low Level rf (LLRF) hardware controller [11,12]. This is possible as each rf station has a dedicated LLRF controller to ensure that the cavity field is synchronized to each individual bunch, within the level of amplitude and phase jitter specified in Table I. The timing system distributes all phase references to the rf stations ensuring the synchronicity across the entire facility [13]. Furthermore, in order to compensate for slow temperature drifts affecting the real

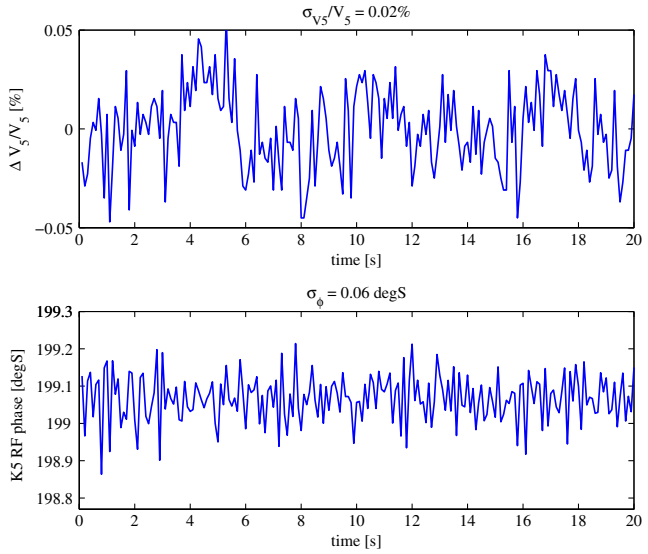

FIG. 6. The relative rf amplitude (top) and rf phase jitter (bottom) of the K5 klystron in L1 rf section measured over 20 sec at a 10 Hz sample rate (feedback active).

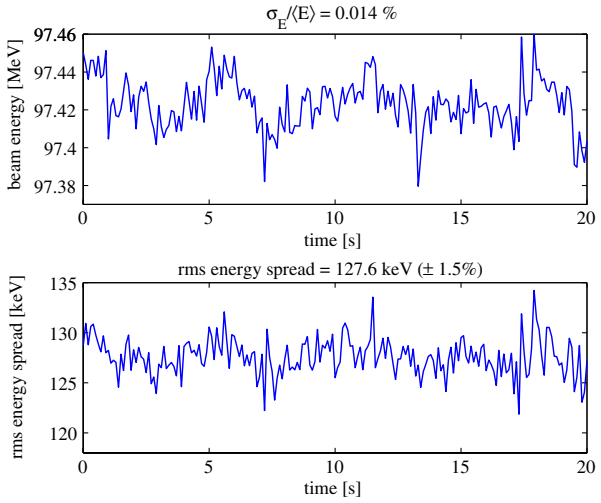

FIG. 7. The bunch mean energy jitter (top) and bunch rms energy spread (bottom) at the injector exit measured over 20 sec at a 10 Hz sample rate.

time measurements of the rf signals from the accelerating structures, a calibration signal is sent between pulses to measure the phase drift in the cables and compensate for it with a digital processing. Afterwards the rf signals are down-converted by means of a rf analog front end to a 99 MHz intermediate frequency (IF) then digitalized at 121×10^6 samples per second (MSPS) by high performance 14 bits analog-to-digital converters (ADCs), acquiring the sine waveform during the rf pulse. A Spartan-3 Field Programmable Gate Array (FPGA) based digital controller converts the digitalized sine waveform into the equivalent amplitude and phase values and locks the local rf phase to the reference phase provided by the timing distribution system and applies the correction needed to compensate for the drifts along the optical cables.

The measured phase and amplitude are also used in feedback loops to control the output rf pulse. The phase loop process makes the difference between cavity and reference phases and the deviation from the set point is summed to the following generated pulse phase. The amplitude loop process makes the difference between cavity and set point amplitude and its gain is set to recover from a step variation within 20 pulses (0.4 sec at 50 Hz). The amplitude and phase loop output values are then used to generate the digitalized pulsed sine waveform which, after a digital-to-analog conversion, is up-converted by the analog front end [14,15]. The rf front end adds a phase noise of 0.0005 degS and 0.0025 degS in down and up conversions, respectively [16] while the local clock time jitter is lower than 20 fsec rms. Thus the overall noise of the entire system is approximately 0.019 degS in phase and 0.018% in amplitude.

The ATJ after BC1 is measured with the bunch arrival monitor (BAM), based on an original idea developed at FLASH/DESY [17] and specifically designed and built inhouse for FERMI [18]. The bunch arrival time is identified by the relative measurement of the electrical signal produced by the bunch when it passes through the pickup mounted on the beam line and the optical pulsed timing [13] taken as a reference signal. This kind of measurement can be considered an experimental proof of the relative stability between the pulsed timing (feeding the photoinjector laser and the BAM station after BC1) and the reference of the rf plants including the whole synchronization chains. The pickup signal is fed to a commercial 12 GHz Mach-Zehnder type electro-optical modulator, and it is utilized to modulate the amplitude of one of the laser pulse trains of the timing reference. The bunch ATJ moves the temporal position of the slope and thus the laser pulse experiences an amplitude modulation. In this way, amplitude variations of the laser pulse train can be correlated to the ATJ. Figure 8 shows the spread of the arrival-time measured over 50 bunches at the nominal compression factor, which corresponds to 115° in the linac 1. The resolution of the BAM system depends on the slope of the modulating signal coming out from the pick up, on the amplitude noise of the optical sampling pulse and of course on the noise of the electronic acquisition system. We have estimated the resolution from the noise floor measurement of the full chain (when the beam was not present, i.e., without optical modulation process) and from the BAM calibration factor measured with the beam. The resolution obtained with the BAM prototype setup at the time of the measurements was around 20 fs.

As shown in Table I, a short-term stability of 0.06° has been achieved for each rf plant of linac 1. In order to study the ATJ behavior, we enhanced this value in K3 and K5 to 0.15°, 0.3°, and 0.7°, respectively. Figures 9 and 10 show good agreement between the experimental results and the expected analytical ATJ versus the linac 1 rf phase. In the

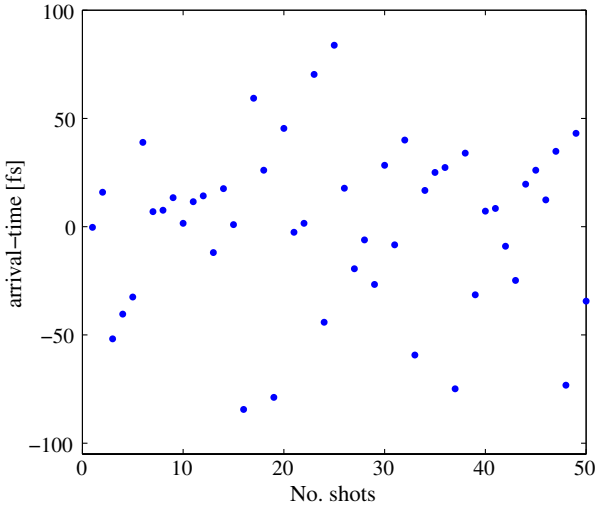

FIG. 8. Spread of the measured arrival time of 50 bunches after the bunch compressor at nominal compression factor. The rms arrival-time jitter for this case is 38 fs.

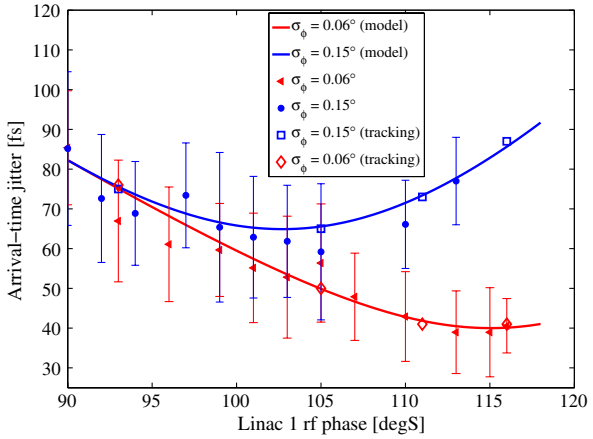

FIG. 9. Measurements, theoretical and numerical expectation of the ATJ versus linac phase for a rf phase jitter of 0.06° and 0.15° . $R_{56} = -41$ mm, Δt_i from the injector is 80 fs (rms).

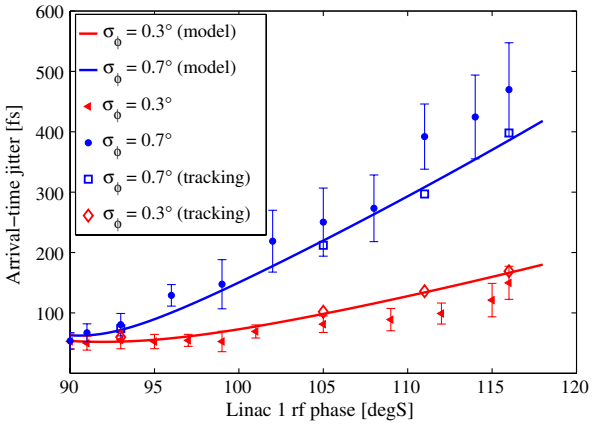

FIG. 10. Measurements, theoretical and numerical expectation of the ATJ versus linac phase for a rms rf phase jitter of 0.3° and 0.7°. $R_{56} = -41$ mm, Δt_i from the injector is 60 fs (rms).

analytical model we assumed a relative amplitude jitter for linac 1 of 0.02% and a chicane $|R_{56}|$ rms jitter of 0.02%. In order to improve the statistics we calculated the mean value of 50 consecutive measurements executed by evaluating the rms ATJ over 1 s, i.e., 10 shots. A local minimum of ATJ occurs for the rf phase of 102° ($C \sim 1.8$), while the rf phase jitter is 0.15°. This minimum moves towards compression factor 1 for larger rf phase jitters. As a conclusion the final arrival-time jitter shrank below 50 fs rms after fixing the jitter sources within the level reported in Table I.

VI. CONCLUSION AND DISCUSSION

The arrival-time jitter of an electron bunch after magnetic compression has been measured in the FERMI@Elettra main linac. The experimental results are well described by an analytical approach that includes the photoinjector laser time jitter, jitter of the phases, and voltages of the radio-frequency accelerator and fluctuations of the compressor's dipole field. The analysis was also successfully benchmarked with particle tracking. Basically, the short-term stability tolerances for the FERMI linac have been achieved for each rf system and consequently the final arrival-time jitter results in being smaller than 50 fs rms. In order to experimentally investigate the ATJ behavior as a function of the rf phase in the linac 1 and hence the compression factor, we systematically added artificial noise to the rf signal by means of the linac 1 low level rf hardware controller. From the analytical model and the measurements we observed a characteristic local minimum in the ATJ versus the rf phase that gradually moved towards smaller compression factors for larger rf phase jitters. This effect was more evident in the presence of a small injector exit time jitter, so that the requirement on the rf phase stability became even more stringent in this case. Local minimum was still observable increasing the level of the linac amplitude jitter but, in that case, the position of the minimum relative to the compression factor was only influenced by the levels of the rf phase jitter and the ATJ at the injector exit jitters. In conclusion we described an experimental methodology that can be generalized to every linac that adopts magnetic chicanes to longitudinally compress the electron beams, where an unexpected too large time jitter is measured. The observation of a local minimum or a monotonic increment of the ATJ when the compression factor is increased has been proved to be a clear signature of a too large jitter in the rf phase of the upstream linac. On the contrary if the ATJ is higher than expected but independent from the compression factor, the main source has to be searched in the dipole current and/or in the upstream linac voltage jitters.

ACKNOWLEDGMENTS

We thank William Fawley and Mauro Predonzani for discussions and suggestions about writing this work. This work was supported in part by the Italian Ministry of University and Research under Grants No. FIRB-RBAP045JF2 and No. FIRB-RBAP-6AWK3.

[1] E. Allaria *et al.*, Nat. Photonics **6**, 699 (2012).
[2] P. Sigalotti *et al.*, Proc. SPIE Int. Soc. Opt. Eng. **8778**, 87780Q (2013).
[3] S. Di Mitri *et al.*, Nucl. Instrum. Methods Phys. Res., Sect. A **608**, 19 (2009).
[4] G. Penco *et al.*, JINST **8**, P05015 (2013).
[5] P. Castro, Report No. DESY-TECH-NOTE-2003-01, 2003.
[6] H. Schlarb, *Proceedings of the 21st Particle Accelerator Conference, Knoxville, 2005* (IEEE, Piscataway, NJ, 2005).
[7] K. Bane and P. Emma, *Proceedings of the 21st Particle Accelerator Conference, Knoxville, 2005* (IEEE, Piscataway, NJ, 2005), p. 4266.

[8] M. Budiman, Matlab utility: Latin Hypercube Sampling, budiman@acss.usyd.edu.au, 2004.
[9] P. Craievich *et al.*, *Proceedings of the 10th European Particle Accelerator Conference, Edinburgh, Scotland, 2006* (EPS-AG, Edinburgh, Scotland, 2006).
[10] S. Di Mitri *et al.*, *Proceedings of the 32nd Free Electron Laser Conference, Malmö, Sweden* (Max-lab, Sweden, 2010).
[11] J. Byrd *et al.*, *Proceedings of the 22nd Particle Accelerator Conference, Albuquerque, New Mexico* (IEEE, New York, 2007).
[12] A. Rohlev *et al.*, *Proceedings of the 11th European Particle Accelerator Conference, Genoa, 2008* (EPS-AG, Genoa, Italy, 2008).
[13] M. Ferianis *et al.*, *Proceedings of the 14th Beam Instrumentation Workshop, Santa Fe, New Mexico, 2010* (LANL, Los Alamos, 2010).
[14] L. Doolittle *et al.*, in *2011 LLRF Workshop,* (DESY, Hamburg, Germany, 2011) [https://indico.desy.de//event/3391].
[15] M. Milloch *et al.*, in Ref. [14].
[16] A. Rohlev *et al.*, in Ref. [14].
[17] F. Löhl *et al.*, Phys. Rev. Lett. **104**, 144801 (2010).
[18] L. Pavlovic *et al.*, *Proceedings of the 14th Beam Instrumentation Workshop, Santa Fe, New Mexico, 2010* (LANL, Los Alamos, 2010).